

# Multistate folding of a hyperthermostable Fe-superoxide dismutase (TcSOD) in guanidinium hydrochloride: The importance of the quaternary structure

Sha Wang<sup>a</sup>, Wei-Feng Liu<sup>b</sup>, Yong-Zhi He<sup>a</sup>, Ao Zhang<sup>b</sup>, Li Huang<sup>a,\*</sup>,  
Zhi-Yang Dong<sup>a,\*</sup>, Yong-Bin Yan<sup>b,\*</sup>

<sup>a</sup> State Key Laboratory of Microbial Resources, Institute of Microbiology, Chinese Academy of Sciences, Beijing 100081, China

<sup>b</sup> State Key Laboratory of Biomembrane and Membrane Biotechnology, Department of Biological Sciences and Biotechnology, Tsinghua University, Beijing 100084, China

Received 2 July 2007; received in revised form 15 November 2007; accepted 3 December 2007

Available online 14 December 2007

## Abstract

Superoxide dismutases (SODs), which are the first line of cellular defense against the toxic effects of reactive oxygen species, are metalloenzymes that catalyze the disproportionation of superoxide radicals to produce oxygen and hydrogen peroxide. Although much effort has been devoted to the folding mechanisms of Cu/Zn-SODs, little is known about the folding of Fe-SODs. In this research, the equilibrium unfolding and refolding of TcSOD, a tetrameric hyperthermostable Fe-SOD, were investigated by circular dichroism, intrinsic fluorescence, ANS fluorescence, size-exclusion chromatography and cross-linking experiments. The results herein suggested that the guanidine hydrochloride-induced unfolding of TcSOD involved a stable monomeric intermediate and a possible tetrameric intermediate. The Gibbs free energy of TcSOD dissociation was about 3-fold larger than that of the monomeric intermediate unfolding, which suggested that the quaternary structure plays a crucial role in TcSOD stability. A comparison of the thermodynamic parameters between TcSOD and other SODs also suggested that the stability of quaternary structure might be responsible for the hyperthermostability of TcSOD.

© 2007 Elsevier B.V. All rights reserved.

**Keywords:** Fe-superoxide dismutase; Hyperthermostable; Protein unfolding and refolding; Folding intermediate; Metalloenzyme

## 1. Introduction

Reactive oxygen species (ROS) are generated as toxic byproducts of normal cellular metabolism, and superoxide is among the most abundant ROS produced by the mitochondria [1]. ROS can damage cellular macromolecules and has been

related to numerous diseases [1,2]. To protect against these toxic compounds, all organisms have evolved effective response systems and enzymes of antioxidative defense. Superoxide dismutases (SODs, EC 1.15.1.1), which are the first line of cellular defense against the toxic effects of ROS [3], are metalloenzymes that catalyze the disproportionation of superoxide radicals to produce oxygen and hydrogen peroxide through a one-electron redox cycle [4,5]. SODs exist widely in both prokaryotic and eukaryotic organisms [6,7], and can be classified into four types depending on the metal selectivity: Cu/Zn-, Mn-, Fe- and Ni-SOD [8,9]. Among them, Cu/Zn-SOD has been characterized in many organisms from *Escherichia coli* to human beings, while Ni-SOD is a recently characterized species [10]. Cu/Zn-SOD is primarily in cytoplasm [11], and is the most studied one, since more than 100 genetic mutations have been related to amyotrophic lateral sclerosis (ALS) [12]. Mn-SOD is mainly found in eukaryotic mitochondria, while Fe-SOD is prevalently found in prokaryotes [7,13]. Fe- and Mn-SODs share a high homology in the amino acid sequence, have similar

**Abbreviations:** SOD, superoxide dismutase; GdnHCl, guanidinium chloride; SDS-PAGE, sodium dodecyl sulfate polyacrylamide gel electrophoresis; ANS, 1-aniline-8-naphthalenesulfonate; CD, circular dichroism;  $E_m$ , emission maximum wavelength of intrinsic fluorescence; SEC, size-exclusion chromatography; ROS, reactive oxygen species

\* Corresponding authors. Y.-B. Yan is to be contacted at Department of Biological Sciences and Biotechnology, Tsinghua University, Beijing 100084, China. Fax: +86 10 6277 1597. Z.-Y. Dong or Li Huang, State Key Laboratory of Microbial Resources, Institute of Microbiology, Chinese Academy of Sciences, Datun Road, Chaoyang District, Beijing 100081, China.

E-mail addresses: [huangl@sun.im.ac.cn](mailto:huangl@sun.im.ac.cn) (L. Huang), [dongzy@sun.im.ac.cn](mailto:dongzy@sun.im.ac.cn) (Z.-Y. Dong), [ybyan@tsinghua.edu.cn](mailto:ybyan@tsinghua.edu.cn) (Y.-B. Yan).

three-dimensional structures, and are supposed to have a common origin different from Cu/Zn-SOD [14,15].

Many Fe-SODs from hyperthermophiles (for example, *Aquifex pyrophilus*, *Sulfolobus solfataricus*, *Sulfolobus acidocaldarius* and *Pyrobaculum aerophilum*) have been purified and characterized [9,16,17], and the three-dimensional structures of several Fe-SODs have been solved to analyze the structural basis for their thermostability [15,16,18]. Unlike the thoroughly studied Cu/Zn-SOD [19–25], little is known about the folding mechanisms and pathways of Fe- or Mn-SOD. In this research, TcSOD, a newly characterized hyperthermophilic Fe-SOD from Tengchong, China [26], was used as a model protein to investigate the unfolding pathway of tetrameric Fe-SOD. TcSOD has about 80% sequence homology with the thermostable Fe-SOD from *A. pyrophilus* (ApSOD) [15,17] and its thermostability is similar to ApSOD [26]. The results herein suggested that the guanidine hydrochloride (GdnHCl)-induced unfolding of TcSOD involved a stable monomeric intermediate and a possible tetrameric intermediate. When the unfolding transition was fitted to a three-state process, the Gibbs free energy of TcSOD dissociation was much higher than that of the monomeric intermediate unfolding, which suggested that the quaternary structure plays a crucial role in TcSOD stability. A comparison of the unfolding mechanisms between TcSOD and other SODs indicated that the dissociation of the TcSOD was about 6kcal/mol larger than that of HSOD or PISOD [20–22]. This suggested that the stability of the quaternary structure might be responsible for the hyperthermostability of TcSOD.

## 2. Materials and methods

### 2.1. Chemicals

GdnHCl, 8-anilino-1-naphthalenesulfonic-acid (ANS) and sodium dodecyl sulfate (SDS) were purchased from Sigma Chemical Co. All other chemicals were local products of analytical grade.

### 2.2. Expression and purification of the recombinant TcSOD

TcSOD was expressed in *E. coli* BL21 with pET28a plasmid and purified by Ni-NTA affinity chromatography as described previously [26]. The SOD activity was measured according to the pyrogallol method [27]. The purity of the final products was above 99% estimated according to SDS-PAGE and size exclusion chromatography analysis. The protein concentrations were determined by the Bradford method using bovine serum albumin as a standard [28]. The SOD activity was defined as the amount of enzyme that inhibits the autoxidation of pyrogallol by 50%. The metal content of TcSOD was measured by atomic absorption spectrophotometer or inductively coupled plasma high resolution mass spectrometry at the Analytical Center of Tsinghua University using a protein concentration of about 0.1mg/ml [26].

### 2.3. Unfolding and refolding of TcSOD

The unfolding of TcSOD was performed by incubating the purified protein in 50 mM Tris-HCl buffer, pH 7.4, containing different concentrations of GdnHCl for 12 h at 4 °C. As for the refolding experiments, the purified TcSOD was first completely denatured with 6 M GdnHCl for 12 h. Then the equilibrium refolding was carried out by dilution of the denatured samples with refolding buffer (50 mM Tris-HCl, pH 7.4) at 25 °C for 24 h. The final concentrations of GdnHCl varied from 0.4–5.8 M. The final concentration of the protein was 0.33 mg/ml for both the unfolding and refolding experiments. The residual or recovered enzymatic activity was measured at 25 °C.

### 2.4. Size-exclusion chromatography

The size-exclusion chromatography (SEC) analysis of the samples was the same as described previously [29]. In brief, gel filtration experiments were carried out on a Superdex 200HR 10/30 column on an AKTA FPLC (Amersham Pharmacia Biotech, Sweden). The column was pre-equilibrated with sodium phosphate buffer (20 mM, pH 7.4) containing the given concentrations of GdnHCl, and then about 100  $\mu$ l protein solutions were injected into the column. All samples were run at a flow rate of 0.5 ml/min at 16 °C.

### 2.5. Spectroscopic experiments

All spectroscopic experiments were performed at 25 °C with a protein concentration of 0.33 mg/ml. Details regarding the spectroscopic experiments were the same as those described previously [29,30]. The circular dichroism (CD) spectra were recorded on a Jasco J-710 spectropolarimeter (Jasco Corp., Tokyo, Japan) with a 1mm pathlength cell over a wavelength range of 190–250 nm. The resultant spectra were obtained by the subtraction of the control. The fluorescence spectra were measured on an F-2500 fluorescence spectrophotometer (Hitachi Ltd., Tokyo, Japan) with a 5-nm slit width for both excitation and emission. The intrinsic fluorescence was measured with an excitation wavelength of 290 nm and an emission wavelength ranging from 300 to 400 nm. The ANS binding affinity to TcSOD at various concentration of GdnHCl was monitored with an excitation wavelength of 380 nm and an emission wavelength ranging from 400 to 600 nm. The final concentration of ANS was 20  $\mu$ M.

### 2.6. Parameter *A* and phase diagram analysis

Parameter *A*, which is the ratio of the intensity at 320 nm to that at 365 nm of the intrinsic fluorescence ( $I_{320}/I_{365}$ ), is the characteristic of the shape and position of the fluorescence spectrum [31]. Parameter *A* analysis has been successfully used in monitoring protein conformational changes [32,33], and was also used in this research to detect the structural changes of TcSOD during denaturation and renaturation. The phase diagram analysis of the intrinsic fluorescence, which is a sensitive tool to detect folding intermediates, was carried out as described previously [32,34]. In brief, the phase diagram was constructed by the fluorescence intensity at 320 nm versus that at 365 nm at different GdnHCl concentrations. The fluorescence data were normalized by the corresponding intensity of the spectra recorded in buffers without the addition of GdnHCl. In the diagram, a straight line reflects an “all-or-none” process, while the non-linearity between  $I_{320}$  and  $I_{365}$  implies that the structural transition involves folding intermediate(s). For the latter case, the joint position of the two lines indicates that an intermediate appeared at the corresponding concentration of GdnHCl.

### 2.7. Cross-linking experiments by glutaraldehyde

The protein samples were the same as those for protein unfolding studies described above. The cross-linking experiments were conducted by mixing 400  $\mu$ l proteins solutions denatured in various amounts of GdnHCl with 60  $\mu$ l freshly prepared glutaraldehyde solutions. The concentration of the protein was 0.25 mg/ml, while that of glutaraldehyde was 2.3%. The reaction buffer was 20 mM sodium phosphate buffer, pH 7.4. After 5 min treatment at room temperature, the reaction was terminated by the addition of 30  $\mu$ l Tris-HCl with a concentration of 1 M (pH 8.0). Then the samples were dialyzed against 20 mM sodium phosphate buffer (pH 7.4) overnight. Finally, the samples were concentrated to a volume of 300  $\mu$ l with a speed vacuum concentrator (SAVANT, Thermo Life Sciences, USA). The oligomeric states of the proteins were checked by SDS-polyacrylamide gel electrophoresis (SDS-PAGE) using 12.5% separating gel in the reducing conditions.

## 3. Results

First of all, the inactivation of TcSOD induced by GdnHCl was explored by monitoring the residual activity in various amounts of GdnHCl. As presented in Fig. 1, the activity

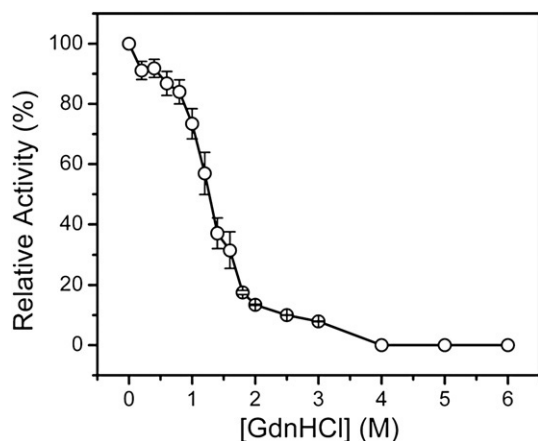


Fig. 1. Inactivation of TcSOD by GdnHCl. The enzyme was dissolved in 50 mM Tris–HCl buffer, pH 7.4, in the presence of increasing concentration of GdnHCl. The final protein concentration was 0.33 mg/ml.

decreased continuously when the enzyme was incubated in buffers in the presence of increasing concentrations of GdnHCl. The enzyme could retain most of its activity (> 90%) when the

GdnHCl concentration was below 0.5 M, while a steep decrease of the enzymatic activity was observed when the GdnHCl concentration was between 0.5 and 1.4 M GdnHCl. The enzyme was almost fully inactivated in about 2 M GdnHCl, and the midpoint of TcSOD inactivation was about 1.2 M GdnHCl. No significant difference was observed for samples with varying enzyme concentrations, which suggested that the inactivation of TcSOD by GdnHCl might be independent of the enzyme concentration. When 6 M GdnHCl-denatured TcSOD was refolded in buffers containing 0.4 M GdnHCl at room temperature for 24 h, about 50% activity could be recovered (data not shown), indicating that the folding of TcSOD in GdnHCl was more like to be partially reversible.

CD, intrinsic and extrinsic fluorescence were performed to monitor the secondary and tertiary structural changes during TcSOD folding. As presented in Fig. 2A, the change of the secondary structure was an obvious two-stage process with increasing concentrations of GdnHCl. The first transition appeared from 1.8 M to 2.8 M GdnHCl, while the second occurred from 4.0 M to 5.2 M GdnHCl. This observation suggested that a stable unfolding intermediate existed at GdnHCl concentrations

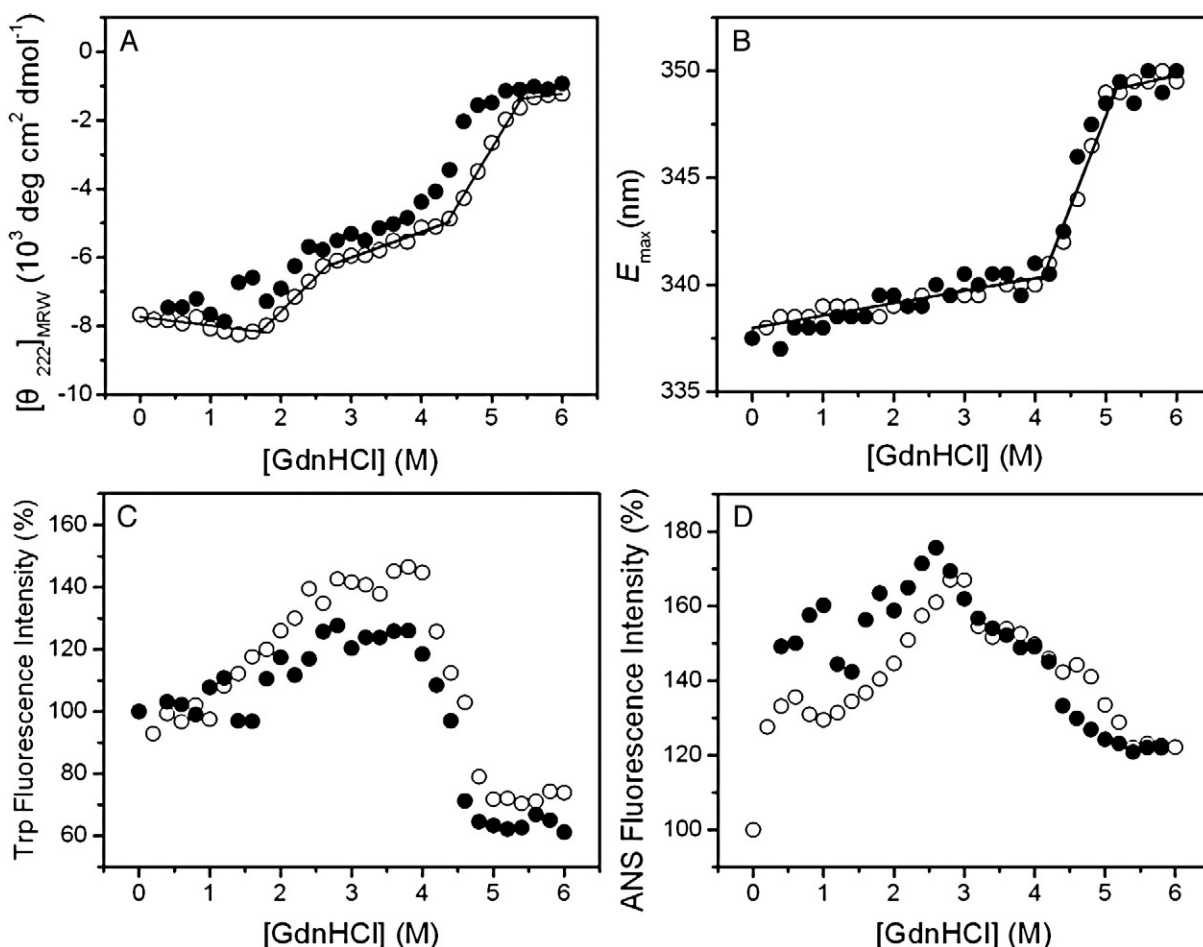


Fig. 2. Unfolding (open symbols) and refolding (filled symbols) of TcSOD monitored by the ellipticity at 222 nm (A), the emission maximum wavelength (B) and intensity (C) of the intrinsic fluorescence, and ANS fluorescence intensity at 470 nm (D). The data in panels A and B were fitted by the equations listed in Table 1 and the fitting results are presented as solid lines. For the unfolding experiments, the protein was incubated in 50 mM Tris–HCl buffer, pH 7.4, in the presence of various concentrations of GdnHCl for 12 h at 4 °C. For the refolding experiments, the protein was fully denatured in 6 M GdnHCl for 12 h, and then equilibrium refolding was achieved by dilution of the fully-denatured protein into the refolding buffer (50 mM Tris–HCl, pH 7.4) containing 0.4–5.8 M GdnHCl. The final protein concentration was 0.33 mg/ml. All spectroscopic experiments were carried out at 25 °C.

of around 3.5 M. The recovery of the secondary structure also revealed a similar two-stage process with the accumulation of a refolding intermediate. The minor deviation between the two curves suggested that the folding of TcSOD was mainly reversible, which is consistent with the activity results described above.

The emission maximum wavelength of the intrinsic fluorescence ( $E_{\max}$ ) of the native TcSOD was found to be about 337.5 nm, which suggested that most of the Trp residues in TcSOD were exposed to bonded waters [32,33,35]. This observation is consistent with the modeling structure of TcSOD [26]. Different from the three-state unfolding reflected by the CD result (Fig. 2A), the change of the emission  $E_{\max}$  was more like a two-state transition. The emission  $E_{\max}$  red-shifted about 2.5 nm when the GdnHCl concentration was increased from 0 M to 4 M (Fig. 2B), indicating that only minor changes occurred in the microenvironments of the Trp residues. A significant red-shift from 340 nm to 350 nm of the emission  $E_{\max}$  appeared when the protein denatured in 4.2–5.2 M GdnHCl, suggesting that the Trp residues were fully exposed to solvent when the GdnHCl concentration was above 5.2 M. The emission intensity of the intrinsic fluorescence was found to increase at GdnHCl concentrations above 1.8 M, reaching its maximum at ~2.8 M GdnHCl, and decreasing gradually when the GdnHCl concentration was above 4.0 M. This suggested an intermediate might be populated at GdnHCl concentrations of around 3.5 M, which is similar to the results obtained from CD data. Moreover, the refolding data coincided well with that of the unfolding of TcSOD as monitored by intrinsic fluorescence. ANS is a fluorescent probe that has been widely used to monitor the hydrophobic exposure of proteins [36]. As shown in Fig. 2D, the ANS fluorescence intensity at 470 nm increased as the GdnHCl concentration increased, and reached a maximum at about 3.0 M GdnHCl. In addition to the peak at 3.0 M GdnHCl, several small peaks or shoulders could also be identified. However, the overall increase of the ANS fluorescence intensity was less than 1.8-fold of the native protein, which suggested that no significant increase in hydrophobic exposure of TcSOD was induced by the denaturation of GdnHCl.

The dissimilarity in the changes of the emission  $E_{\max}$  value and intensity (Fig. 2B and C) might be caused by the inability of these two analyzing methods to reflect the change of the shape of the intrinsic fluorescence spectra. To more precisely characterize the folding transitions of TcSOD, the intrinsic fluorescence spectra were further analyzed by parameter  $A$  and phase diagram. Parameter  $A$ , which is obtained by the dividing of the intensity at 320 nm by that at 365 nm, has long been used to reflect the shape and position of the Trp fluorescence spectra [31,33]. As shown in Fig. 3A, the parameter  $A$  data indicated that the change of the intrinsic fluorescence was a typical three-state process with an intermediate accumulated at GdnHCl concentrations between 2.8 M and 3.8 M. Furthermore, the phase diagram, a sensitive tool to characterize the folding intermediate(s) [32,34], was constructed by monitoring the change of the intensity at 365 nm as a function of that at 320 nm (Fig. 3B). Two linear parts, corresponding to GdnHCl concentrations of about 0–3.0 and 4.0–6.0 M, respectively,

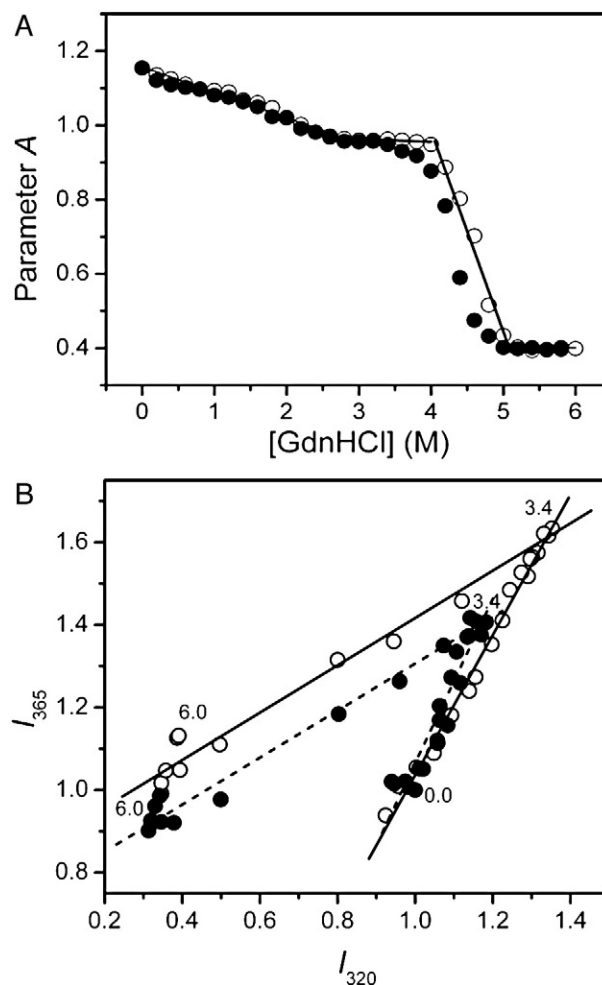


Fig. 3. Parameter  $A$  (A) and phase diagram (B) analysis of the intrinsic fluorescence spectra of TcSOD during unfolding (open symbols) and refolding (filled symbols). The parameter  $A$  was obtained by dividing the fluorescence intensity at 320 nm ( $I_{320}$ ) by that at 365 nm ( $I_{365}$ ). The phase diagram was constructed by monitoring the changes of  $I_{365}$  as a function of  $I_{320}$ . The solid line in panel A represents the curve fitting results using the equations listed in Table 1.

could be identified for both the unfolding and refolding transitions. Thus the phase diagram analysis also suggested that a stable intermediate was populated during the folding of TcSOD.

To determine the dissociation of TcSOD during GdnHCl-induced unfolding, size-exclusion chromatography (SEC) analysis and cross-linking by glutaraldehyde was performed for samples in the presence of increasing concentration of GdnHCl. The typical SEC profiles are presented in Fig. 4A, and the changes of the peak position and area are summarized in Fig. 4C and D. Native TcSOD mainly existed as a tetramer with a molecular weight of about 112 kDa, which is confirmed by the glutaraldehyde cross-linking experiments (Fig. 4B). It eluted as a single peak centered at 13.0 ml in the SEC profile (Fig. 4A), which is consistent with the previous observation [26]. With the increase of GdnHCl concentration, the elution volume of the native protein decreased slightly (about 0.2 ml).

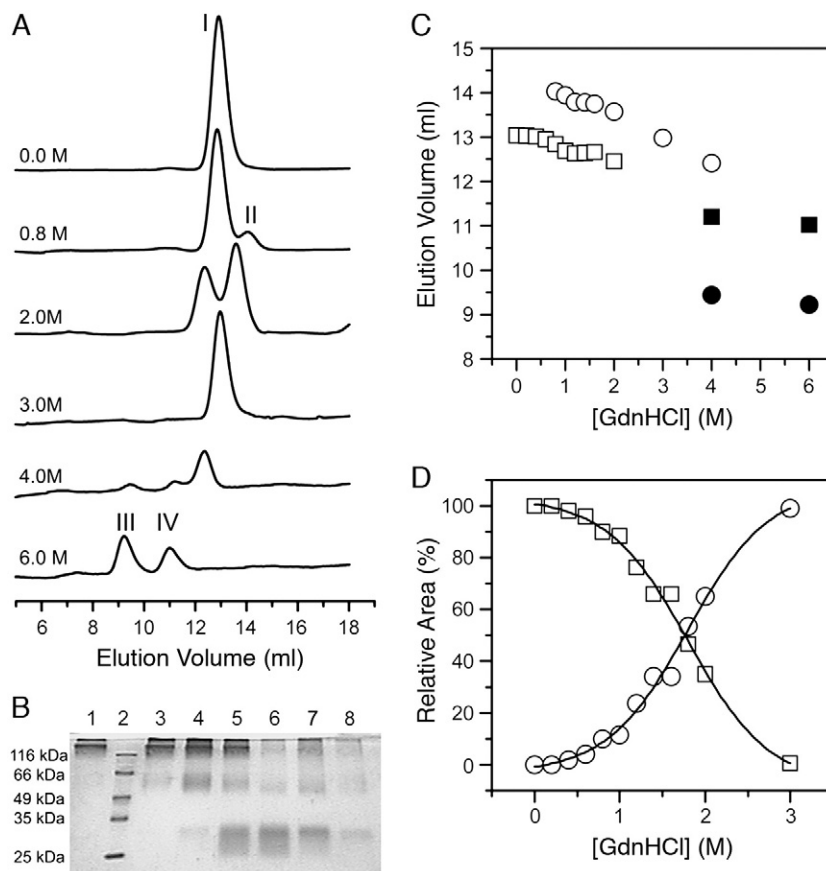


Fig. 4. TcSOD unfolding characterized by SEC and SDS-PAGE analysis. (A) The elution profiles of TcSOD denatured in 0.0, 0.8, 2.0, 3.0, 4.0 and 6.0 M GdnHCl, respectively. Peaks I–IV correspond to the native protein, the monomeric intermediate and two fully-unfolded states. The final protein concentration was 0.33 mg/ml. (B) Dissociation of TcSOD during GdnHCl-induced unfolding monitored by SDS-PAGE of the cross-linked protein by glutaraldehyde. Lanes 1 and 3–8 show the samples pretreated with the cross-linking reagent glutaraldehyde containing 0, 1, 2, 3, 4, 5 and 6 M GdnHCl, respectively. Lane 2 is the protein standards:  $\beta$ -galactosidase from *E. coli* (116 kDa), serum albumin from bovine (66 kDa), ovalbumin from chicken egg white (45 kDa), lactate dehydrogenase from porcine muscle (35 kDa), and REase Bsp981 from *E. coli* (25 kDa). (C) Change of the elution volumes of peak I (open squares), II (open circles), III (filled circles) and IV (filled squares) marked in panel A. (D) Relative areas of peak I (open squares) and II (open circles) as a function of GdnHCl concentration.

Meanwhile, a new peak at about 14 ml appeared when the GdnHCl concentration was above 0.8 M. In 3.0 M GdnHCl, the peak corresponding to the native TcSOD totally disappeared and a single peak eluted at 13.0 ml was observed. The cross-link experiments suggested that a stable monomeric intermediate was populated at this GdnHCl concentration (Fig. 4B). Moreover, as shown in Fig. 4D, the dissociation of the native TcSOD was accompanied with the formation of this monomeric intermediate. A similar tetramer to monomer transition could also be characterized by the cross-linking experiments over the GdnHCl concentration ranging from 2.0 M to 4.0 M. It is worthy noting that the bands over 200 kDa existed in the gel might be formed by the non-specific intermolecular cross-linking of the TcSOD monomers. A band centered at around 56 kDa, which is corresponded to the dimeric form, was observed for samples denatured in all GdnHCl concentrations probably resulted from the GdnHCl dependence on the efficiency of the cross-linking reaction. This deduction was confirmed by the fact that no dimeric intermediate could be characterized from the SEC and spectroscopic experiments.

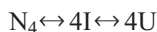
The spectroscopic experiments (Fig. 2) indicated that the protein was fully denatured when the GdnHCl concentration reached 6.0 M. However, two peaks could be identified with different elution volumes (11.0 ml and 9.2 ml). Meanwhile, the protein was dominated by the monomeric form as observed in the SDS-PAGE of the cross-linked sample. Thus the appearance of the two peaks in the SEC profile suggested that the 6.0 M GdnHCl-denatured protein might exist in two distinct states. The metal content of the purified TcSOD was about 0.516 atom per subunit, while it was about 0.404 atom per subunit for the 6.0 M GdnHCl-denatured state as measured by inductively coupled plasma high resolution mass spectrometry. The native protein contained a relative lower iron content compared to the optimal value of 1 atom per subunit, which was caused by the loss of iron during dialysis, purification or storage [26]. The loss of the coordinated metal ions during purification has also been observed in ApSOD [15,17], which suggested that the iron ion was not tightly associated with Fe-SOD. Nevertheless, the data suggested that iron could bind to the fully-denatured state of TcSOD with a similar affinity to the native state. Thus it is possible that the two peaks

in the SEC profile of TcSOD in 6.0 M GdnHCl were in different metal coordination state.

## 4. Discussion

### 4.1. Folding of TcSOD involves a stable monomeric intermediate

The existence of a stable monomeric intermediate has been characterized in the folding of many multimeric proteins [37–41], while the lack of the population of any monomeric forms has also been observed [21,30,42]. As for the tetrameric TcSOD, although the changes of the emission  $E_m$  revealed an apparent two-state transition (Fig. 2B), the change of the CD signal (Fig. 2A) was found to be a typical three-state process during the GdnHCl-induced unfolding and refolding. The dissimilarity between the emission  $E_m$  and CD curves strongly suggested that an intermediate state was populated during TcSOD folding. This conclusion was further verified by the more sensitive Trp fluorescence analytical methods (Fig. 3). The spectral analysis indicated that the intermediate state was mainly accumulated between 2.8 and 3.8 M GdnHCl. The SEC and cross-linking experiments indicated that this intermediate was in a monomeric state (Fig. 4). Thus the folding of TcSOD could be described as a two-step process



where  $N_4$  is the native tetrameric protein [26], I is the monomeric intermediate, and U is the fully-denatured state. The dissociation

Table 2

Thermodynamic parameters of the three-state unfolding of TcSOD

Protein	Probe	$\Delta G_{NI}^{H_2O}$ (kcal/ mol)	$m_{NI}$ (kcal/ mol M)	$\Delta G_{IU}^{H_2O}$ (kcal/ mol)	$m_{IU}$ (kcal/ mol M)	$\Delta G_{NU}^{H_2O}$ (kcal/ mol)
TcSOD	CD	18.3±0.3	3.6±0.2	6.2±0.3	1.3±0.06	43±2
	$E_{max}$	n.d.	n.d.	7.0±0.2	1.5±0.1	n.d.
	Parameter A	12.4±0.6	1.4±0.1	8.0±0.4	1.8±0.1	44±2
PISOD [20]		11.9±0.5	2.9±0.2	5.4±0.5	1.2±0.1	22.7±1.5
HSOD [21]		11.8±0.5	0.86±0.05	8.4±0.5	1.8±0.1	28.6±0.7

n.d.: not determined.

of the  $N_4$ , the formation of I (Fig. 4D), and the loss of enzymatic activity (Fig. 1) were found to be synchronous, which suggested that the tetrameric structure was essential for the efficient catalysis of TcSOD. This observation coincided with the structural study results that a large substrate entry is formed by the subunits of TcSOD or ApSOD [15,26].

The data in Figs. 2A, B and 3A were used for the calculation of the Gibbs free energy of TcSOD unfolding using the equations listed in Table 1. Since GdnHCl-induced denaturation monitored by the  $E_m$  of the intrinsic fluorescence was an apparent two-state process, the Gibbs free energy of the dissociation of the native protein ( $\Delta G_{NI}^{H_2O}$ ) was more reliable when obtained from the transition monitored by CD spectroscopy. The free energy of the unfolding of the monomeric intermediate ( $\Delta G_{IU}^{H_2O}$ ) obtained from the  $E_m$  of the intrinsic fluorescence was similar to that from

Table 1

Equations used for the fitting of the equilibrium unfolding of TcSOD to a three-state model

$N_4 \leftrightarrow 4I$	$4I \leftrightarrow 4U$	
$f_i + f_N = 1$	$f_U + f_I = 1$	1
$f_i = \frac{[I]}{P}$	$f_I = \frac{[I]}{P}$	2
$f_N = \frac{4[N_4]}{P}$	$f_U = \frac{[U]}{P}$	3
$K_{NI} = \frac{[I]^4}{[N_4]} = \frac{4P^3 f_i^4}{1 - f_i}$	$K_{IU} = \frac{[U]}{[I]} = \frac{f_U}{1 - f_U}$	4
$f_i = \frac{y - y_N}{y_I - y_N}$	$f_U = \frac{y - y_I}{y_U - y_I}$	5
$\Delta G_{NI} = -RT \ln K_{NI} = -RT \ln \left( \frac{4P^3 f_i^4}{1 - f_i} \right)$	$\Delta G_{IU} = -RT \ln K_{IU} = -RT \ln \left( \frac{f_U}{1 - f_U} \right)$	6
$\Delta G_{NI} = \Delta G_{NI}^{H_2O} - m_{NI} [\text{GdmHCl}]$	$\Delta G_{IU} = \Delta G_{IU}^{H_2O} - m_{IU} [\text{GdmHCl}]$	7
$\Delta G_{NU}^{H_2O} = \Delta G_{NI}^{H_2O} + 4\Delta G_{IU}^{H_2O}$		8

Abbreviations used are:  $N_4$ , native tetrameric TcSOD; I, monomeric intermediate; U, unfolded state.  $y_N, y_I, y_U$  are the measured signals of each species, while  $f_N, f_I, f_U$  are the corresponding fractional amplitudes.

the CD, suggesting that the change in the intrinsic fluorescence mainly reflected the I  $\leftrightarrow$  U transition. Importantly, the  $\Delta G_{NI}^{H_2O}$  value in the absence of GdnHCl (Table 2), which implied that the quaternary structure provided the main contribution to the stability of TcSOD against GdnHCl denaturation. The coefficients of GdnHCl concentration dependence of the N<sub>4</sub>  $\leftrightarrow$  4I transition ( $m_{NI}$ ) was also found to be about 3-fold larger than that of the I  $\leftrightarrow$  U transition ( $m_{IU}$ ), suggesting that the amount of protein surface exposed to solvent upon unfolding is greater for the I  $\leftrightarrow$  U transition [43]. Moreover, The  $\Delta G_{NU}^{H_2O}$  values calculated by CD and parameter *A* data were coincident, which was nearly 2-fold larger than those of PISOD and HSOD [20,21]. The two characteristic concentrations of GdnHCl,  $f_N^{-1}(0.5)$ , at which half of the TcSOD were dissociated into monomer intermediates, and  $f_U^{-1}(0.5)$ , at which half of the intermediates were unfolded, were calculated from Eq. 7 and were 2.2 M and 4.6 M, respectively. It is worth noting that the midpoint of TcSOD inactivation by GdnHCl was  $1.3 \pm 0.1$  M when the data in Fig. 1 were fitted to a two-state model. This value was smaller than the calculated  $f_N^{-1}(0.5)$  value, which suggested that the inactivation

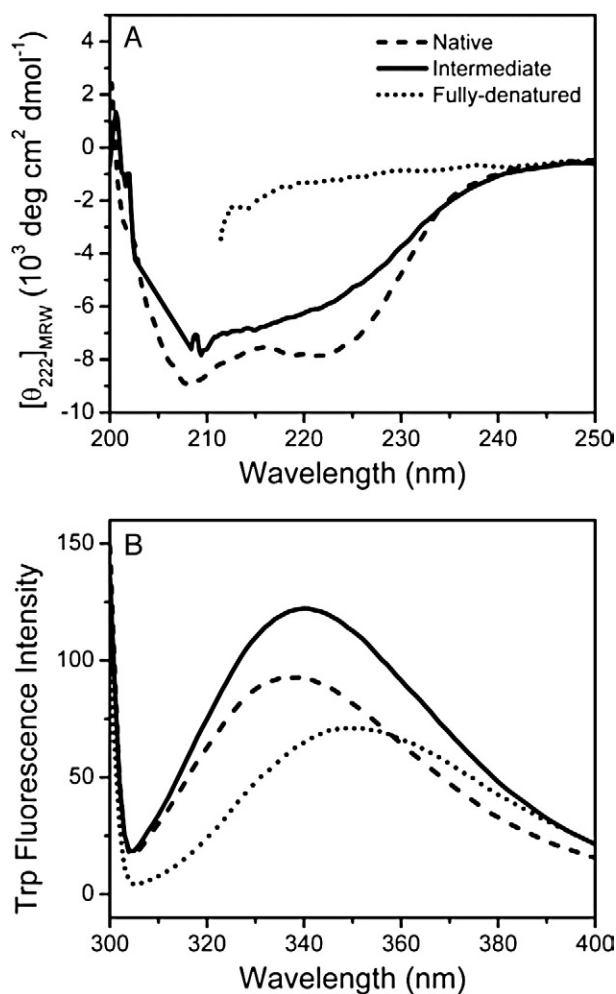


Fig. 5. A comparison of the CD (A) and intrinsic fluorescence (B) spectra of the native state, unfolding intermediate in 3.4 M GdnHCl, and unfolded state in 6 M GdnHCl of TcSOD. Details regarding the sample preparation and spectroscopic experiments were the same as those described in Fig. 2.

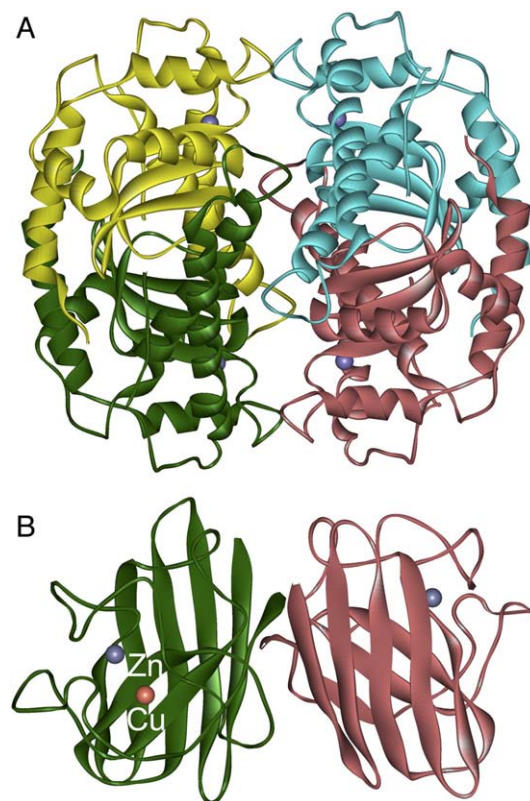


Fig. 6. A comparison of the crystal structures of the hyperthermophilic Fe-SOD from *A. pyrophilus* (A, PDB ID 1COJ) and human Cu/Zn-SOD (B, PDB ID 1HL5).

was prior to the dissociation of TcSOD during GdnHCl-induced unfolding.

#### 4.2. Characteristics of the intermediate and unfolded state

Fig. 5 shows a comparison of the CD and intrinsic fluorescence spectra of the three populated states (N, I and U) during TcSOD unfolding. The ellipticity of the monomeric intermediate was about 70% of the native enzyme (Fig. 5A), indicating that considerable amounts of native secondary structures were maintained in the intermediate. The CD spectrum of the native protein contained two obvious negative peaks at about 208 nm and 222 nm, which was consistent with the findings that the structure of TcSOD is composed of large amounts of  $\alpha$ -helices [26]. However, the CD spectrum of the intermediate indicated that the intermediate was dominated by  $\beta$ -sheet structures. The dissimilarity in the characteristics of the CD spectra between the native and intermediate states suggested that the dissociation might be accompanied by the unfolding of some of the  $\alpha$ -helices of TcSOD. This deduction was also consistent with the fact that the  $\alpha$ -helices contribute to the inter-subunit interactions in TcSOD [15,26].

Structure modeling indicated that TcSOD and *A. pyrophilus* SOD (ApSOD) share a high structural similarity [15,26], and the crystal structure of the tetrameric ApSOD is presented in Fig. 6A. Each subunit of TcSOD is composed of two domains: the N-terminal domain consisting of two long antiparallel

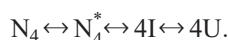
$\alpha$ -helices, and the C-terminal domain containing a central  $\beta$ -sheet surrounded by five  $\alpha$ -helices. Moreover, each subunit has three Trp residues, all of which are located in the C-terminal domain [26]. Among them, Trp110 and Trp191 are located on the helices of the C-terminal domain, and are in a water-accessible microenvironment. Trp127 is located on the first  $\beta$ -strand of the central  $\beta$ -sheet, and is buried in the hydrophobic core of the C-terminal domain. The distinct distribution of these Trp residues provides a sensitive tool in monitoring the structural changes of the C-terminal domain. As shown in Figs. 2 and 5, the intrinsic fluorescence of TcSOD was centered at 337.5 nm, which was close to the value of the fluorophore exposed to bonded water [35]. The small contribution of the Trp in the hydrophobic microenvironment (Trp 127) to the fluorescence of TcSOD suggested that the fluorescence of the Trp127 was partially quenched in the native protein. This deduction was further confirmed by the about 150% intensity increase of the intrinsic fluorescence of the intermediate compared to that of the native state. The emission  $E_m$  of the intermediate was 340 nm, indicating that all the Trp residues in the intermediate were exposed to bonded water. Thus the folding intermediate could be characterized as a state with about 30% decline in native secondary structures and with a less compact structure in the C-terminal domain.

CD experiments (Fig. 2) indicated that the protein lost most of its native secondary structures, and was mainly composed of random coils under the same conditions (Fig. 5). Meanwhile, the emission  $E_m$  of the Trp fluorescence of the 6 M GdnHCl-denatured protein was at about 350 nm, suggesting that most of the Trp residues were fully exposed to solvent [35]. These spectroscopic experiments suggested that TcSOD was fully denatured in 6 M GdnHCl. Interestingly, two distinct peaks were observed in the SEC profile of the protein denatured in 6 M GdnHCl (Fig. 4A). Furthermore, the mass spectrometry analysis indicated that the 6 M GdnHCl-denatured state contains about 0.404 iron per subunit. Thus the existence of two peaks appearing at different elution volumes in the SEC profile implied that the denatured state of TcSOD might be composed of two populated species with different metal coordination states. Further research is in progress to investigate the effects of  $Fe^{2+}$ -coordination on TcSOD folding and stability.

#### 4.3. A tetrameric folding intermediate might exist during the GdnHCl-induced folding of TcSOD

The existence of the multimeric folding intermediate has been characterized in many proteins (for example, [44–47]). A tetrameric intermediate ( $N_4^*$ ) might also exist during the GdnHCl-induced folding of TcSOD. The ellipticity (Fig. 2A) of TcSOD increased slightly in low concentrations of GdnHCl, which implied that structural rearrangement was induced by the chemical denaturant. Similar increase of the CD signal was also observed in the unfolding of other proteins [48,49]. Meanwhile, a peak at around 1.0 M GdnHCl could be identified in the ANS fluorescence data shown in Fig. 2D. A small platform around 1.0 M GdnHCl could also be observed in the Parameter  $A$  data (Fig. 3A). Furthermore, the elution time of the tetrameric native protein (Fig. 4C) revealed a typical two-state process, suggesting that a

tetrameric intermediate with dissimilar molecular volume to the native state might form at GdnHCl concentrations above 1.0 M. It seems that a tetrameric folding intermediate accumulated at about 1.0 M GdnHCl. However, this multimeric state was not as stable as the monomeric intermediate, and was difficult to trap since it appeared at a GdnHCl concentration where the enzyme was in equilibrium in the tetrameric and monomeric states. The reason that this tetrameric intermediate could not be identified by intrinsic fluorescence (Figs. 2B, C and 3) might have been that the low concentrations of GdnHCl had little effects on the structure of the C-terminal domain of TcSOD. This tetrameric state could be characterized as an active state (Fig. 1) with subtle perturbation of the secondary structure compositions (Fig. 2A), an intact C-terminal domain (Fig. 2B and C), slightly loose quaternary structure (Fig. 4C), and  $\sim 150\%$  increase in hydrophobic exposure (Fig. 2D). Then the folding of TcSOD could be described as a four-state process



#### 4.4. Comparison of the folding pathways of TcSOD and other SODs

As mentioned in the introduction, of the four types of SODs, the folding mechanisms of Cu/Zn-SOD are the best studied. Similar to the folding of TcSOD, a stable monomeric intermediate has also been characterized in the folding of Cu/Zn-SOD [19–22,50]. It seems that such a three-state folding mechanism with the appearance of a monomeric intermediate ( $N \leftrightarrow I \leftrightarrow U$ ) was common among the SOD family. However, the properties of the folding intermediate of Fe- and Cu/Zn-SOD are quite different. The folding intermediate of Cu/Zn-SOD is characterized by a minor change in the CD signal and a gradual change in the fluorescence emission [20,21], while that of TcSOD is identified by a minor change in the Trp fluorescence and about 30% decline in the ellipticity (Fig. 2). These differences which might arise from the dissimilarity in their sequence and structure (Fig. 6) [14,15]. The dimeric Cu/Zn-SOD from all species contains a conserved Greek-key  $\beta$ -barrel made up of eight antiparallel  $\beta$ -strands [51,52], while the structure of the tetrameric Fe-SOD is composed of a central  $\beta$ -sheet in the C-terminal domain surrounded by  $\alpha$ -helices [15,26]. It is possible that most of the secondary structures were maintained in the intermediate of the Cu/Zn-SOD. As for TcSOD, the spectroscopic experiments suggested that the unfolding of the helices might occur earlier at low concentrations of GdnHCl, while the unfolding of the central  $\beta$ -sheet might be the final step of TcSOD unfolding. The conclusion that the central  $\beta$ -sheet is crucial for protein stabilization has also been observed in many other proteins (for example, [33,45]).

The quaternary structure is suggested to be crucial to the stability of both Cu/Zn-SOD and Fe-SOD. It has been found that the Gibbs free energy of human Cu/Zn-SOD dissociation was about 2-fold greater than the unfolding of the monomeric intermediate [20]. Similarly, the results herein also indicated that the Gibbs free energy of the  $N_4 \leftrightarrow 4I$  transition was about 3-fold larger than the  $I \leftrightarrow U$  transition. It seems that the quaternary structure provided a

major contribution to the stability of all multimeric SODs. This observation coincided with the proposal that oligomerization is crucial to protein structure, function and stability [40,42,53,54]. Moreover, the monomeric intermediate of TcSOD was populated between 3 M to 3.8 M GdnHCl, while it appeared between 4 M to 5 M GdnHCl for human Cu/Zn-SOD. The values of the thermodynamic parameter of the unfolding of the monomeric intermediate of TcSOD (Table 2) was found to be similar to those of Cu/Zn-SOD from human (HSOD) and *Photobacterium leiognathi* (PISOD), while that of the dissociation of the multimeric protein was about 6 kcal/mol larger than that of HSOD or PISOD [20–22]. This suggested that TcSOD was more stable than the other two SODs, and the quaternary structure was responsible for its high stability. Considering that TcSOD is a hyperthermostable enzyme but HSOD or PISOD are not, it seems that the hyperthermophilic property of TcSOD might be arisen from the stability of its tetrameric structure. The observation that the inter-subunit association is a principal factor for protein stability has also been verified in the hyperthermostable Fe-SOD from *A. pyrophilus* [15] and other proteins [37–42,21,30,45]. As mentioned above, the three-state folding mechanisms might be common among SOD proteins, and the major difference might be the properties of the intermediate state or N $\leftrightarrow$ I transition. It seems that the tight quaternary structure enabled the hyperthermostable Fe-SODs function correctly under extreme environments. Further research is needed to provide a detailed understanding of the structural and folding basis of hyperthermostable SODs.

## Acknowledgements

This investigation was supported by grant 30500084 (to Y.-B. Yan) from the National Natural Science Foundation of China and grant 2004AA214080 (to Z.-Y. Dong) from the National High Technology Research and Development Program (863 project) of China.

## References

- [1] P.S. Brookes, Y.S. Yoon, J.L. Robotham, M.W. Anders, S.S. Sheu, Calcium, ATP, and ROS: a mitochondrial love–hate triangle, *Am. J. Physiol., Cell Physiol.* 287 (2004) C817–C833.
- [2] K.K. Griendling, G.A. FitzGerald, Oxidative stress and cardiovascular injury. Part I: basic mechanisms and in vivo monitoring of ROS, *Circulation* 108 (2003) 1912–1916.
- [3] I. Fridovich, Superoxide radical and superoxide dismutases, *Annu. Rev. Biochem.* 64 (1995) 97–112.
- [4] Y. Takeda, H. Avila, Structure and gene expression of the *E. coli* Mn-superoxide dismutase gene, *Nucleic Acids Res.* 14 (1986) 4577–4589.
- [5] M.B. Yim, P.B. Chock, E.R. Stadtman, Copper, zinc superoxide dismutase catalyzes hydroxyl radical production from hydrogen peroxide, *Proc. Natl. Acad. Sci. U. S. A.* 87 (1990) 5006–5010.
- [6] J.V. Bannister, W.H. Bannister, G. Rotilio, Aspects of the structure, function, and applications of superoxide dismutase, *CRC Crit. Rev. Biochem.* 22 (1987) 111–180.
- [7] A.L. Brioukhanov, A.I. Netrusov, Catalase and superoxide dismutase: distribution, properties, and physiological role in cells of strict anaerobes, *Biochemistry* 69 (2004) 949–962.
- [8] A.-F. Miller, Superoxide dismutases: active sites that save, but a protein that kills, *Curr. Opin. Chem. Biol.* 8 (2004) 162–168.
- [9] M.M. Whittaker, J.W. Whittaker, Recombinant superoxide dismutase from a hyperthermophilic archaeon, *Pyrobaculum aerophilum*, *J. Biol. Inorg. Chem.* 5 (2000) 402–408.
- [10] J.W. Lee, J.H. Roe, S.O. Kang, Nickel-containing superoxide dismutase, *Methods Enzymol.* 349 (2002) 90–101.
- [11] J.D. Crapo, T. Oury, C. Rabouille, J.W. Slot, L. Chang, Copper, zinc superoxide dismutase is primarily a cytosolic protein in human cells, *Proc. Natl. Acad. Sci. U. S. A.* 89 (1992) 10405–10409.
- [12] J.S. Valentine, P.A. Doucette, S.Z. Potter, Copper–zinc superoxide dismutase and amyotrophic lateral sclerosis, *Ann. Rev. Biochem.* 74 (2005) 563–593.
- [13] C.J. Nettleton, C. Bull, T.O. Baldwin, J.A. Fee, Isolation of the *Escherichia coli* iron superoxide dismutase gene: evidence that intracellular superoxide concentration does not regulate oxygen-dependent synthesis of the manganese superoxide dismutase, *Proc. Natl. Acad. Sci. U. S. A.* 81 (1984) 4970–4973.
- [14] T. Hunter, J.V. Bannister, G.J. Hunter, Thermostability of manganese- and iron-superoxide dismutases from *Escherichia coli* is determined by the characteristic position of a glutamine residue, *Eur. J. Biochem.* 269 (2002) 5137–5148.
- [15] J.-H. Lim, Y.G. Yu, Y.S. Han, S.-J. Cho, B.-Y. Ahn, S.-H. Kim, Y. Cho, The crystal structure of a Fe-superoxide dismutase from the hyperthermophile *Aquifex pyrophilus* at 1.9 Å resolution: structural basis for thermostability, *J. Mol. Biol.* 270 (1997) 259–274.
- [16] T. Ursby, B.S. Adinolfi, S. Al-Karadaghi, E. De Vendittis, V. Bocchini, Iron superoxide dismutase from the archaeon *Sulfolobus solfataricus*: analysis of structure and thermostability, *J. Mol. Biol.* 286 (1999) 189–205.
- [17] J.-H. Lim, Y.G. Yu, I.-G. Choi, J.-R. Ryu, B.-Y. Ahn, S.-H. Kim, Y.-S. Han, Cloning and expression of superoxide dismutase from *Aquifex pyrophilus*, a hyperthermophilic bacterium, *FEBS Lett.* 406 (1997) 142–146.
- [18] S. Knapp, S. Kardinal, N. Hellgren, G. Tibbelin, G. Schäfer, R. Ladenstein, Refined crystal structure of a superoxide dismutase from the hyperthermophilic archaeon *Sulfolobus acidocaldarius* at 2.2 Å resolution, *J. Mol. Biol.* 285 (1999) 689–702.
- [19] G. Mei, N. Rosato, N.J. Silva, R. Rusch, E. Gratton, I. Savini, A. Finazzi-Agro, Denaturation of human Cu/Zn superoxide dismutase by guanidine hydrochloride: a dynamic fluorescence study, *Biochemistry* 31 (1992) 7224–7230.
- [20] F. Malvezzi-Campeggi, M.E. Stroppolo, G. Mei, N. Rosato, A. Desideri, Evidence of stable monomeric species in the unfolding of Cu,Zn superoxide dismutase from *Photobacterium leiognathi*, *Arch. Biochem. Biophys.* 370 (1999) 201–207.
- [21] M.E. Stroppolo, F. Malvezzi-Campeggi, G. Mei, N. Rosato, A. Desideri, Role of the tertiary and quaternary structures in the stability of dimeric copper,zinc superoxide dismutases, *Arch. Biochem. Biophys.* 377 (2000) 215–218.
- [22] J.A.O. Rumpf, P.B. Stathopoulos, A. Chakrabarty, J.R. Lepock, E.M. Meiering, Mechanism and thermodynamics of guanidinium chloride-induced denaturation of ALS-associated mutant Cu,Zn superoxide dismutases, *J. Mol. Biol.* 355 (2006) 106–123.
- [23] K.A. Vassall, P.B. Stathopoulos, J.A. Rumpf, J.R. Lepock, E.M. Meiering, Equilibrium thermodynamic analysis of amyotrophic lateral sclerosis-associated mutant apo Cu,Zn superoxide dismutases, *Biochemistry* 45 (2006) 7366–7379.
- [24] A. Nordlund, M. Oliveberg, Folding of Cu/Zn superoxide dismutase suggests structural hotspots for gain of neurotoxic function in ALS: Parallels to precursors in amyloid disease, *Proc. Natl. Acad. Sci. U. S. A.* 103 (2006) 10218–10223.
- [25] M.J. Lindberg, J. Normark, A. Holmgren, M. Oliveberg, Folding of human superoxide dismutase: disulfide reduction prevents dimerization and produces marginally stable monomers, *Proc. Natl. Acad. Sci. U. S. A.* 101 (2004) 15893–15898.
- [26] Y.-Z. He, K.-Q. Fan, C.-J. Jia, Z.-J. Wang, W.-B. Pan, L. Huang, K.-Q. Yang, Z.-Y. Dong, Characterization of a hyperthermostable Fe-superoxide dismutase from hot spring, *Appl. Microbiol. Biotechnol.* 75 (2007) 367–376.
- [27] S. Marklund, G. Marklund, Involvement of the superoxide anion radical in the autoxidation of pyrogallol and a convenient assay for superoxide dismutase, *Eur. J. Biochem.* 47 (1974) 469–474.
- [28] M.M. Bradford, Rapid and sensitive method for the quantitation of microgram quantities of protein utilizing the principle of protein-dye binding, *Anal. Biochem.* 73 (1976) 248–254.

- [29] Y. Jiang, Y.-B. Yan, H.-M. Zhou, Polyvinylpyrrolidone 40 assists the refolding of bovine carbonic anhydrase B by accelerating the refolding of the first molten globule intermediate, *J. Biol. Chem.* 281 (2006) 9058–9065.
- [30] T.-J. Zhao, S. Feng, Y.-L. Wang, Y. Liu, X.-C. Luo, H.-M. Zhou, Y.-B. Yan, Impact of intra-subunit domain–domain interactions on creatine kinase activity and stability, *FEBS Lett.* 580 (2006) 3835–3840.
- [31] K.K. Turoverov, S.Y. Haitlina, G.P. Pinaev, Ultra-violet fluorescence of actin. Determination of actin content in actin preparations, *FEBS Lett.* 62 (1976) 4–6.
- [32] J.-T. Su, S.-H. Kim, Y.-B. Yan, Dissecting the pretransitional conformational changes in aminoacylase I thermal denaturation, *Biophys. J.* 92 (2007) 578–587.
- [33] H.-W. He, J. Zhang, H.-M. Zhou, Y.-B. Yan, Conformational change in the C-terminal domain is responsible for the initiation of creatine kinase thermal aggregation, *Biophys. J.* 89 (2005) 2650–2658.
- [34] N.A. Bushmarina, I.M. Kuznetsova, A.G. Biktashev, K.K. Turoverov, V.N. Uversky, Partially folded conformations in the folding pathway of bovine carbonic anhydrase II: a fluorescence spectroscopic analysis, *ChemBiochem.* 2 (2001).
- [35] Y.K. Reshetnyak, Y. Koshevnik, E.A. Burstein, Decomposition of protein tryptophan fluorescence spectra into log-normal components. III. Correlation between fluorescence and microenvironment parameters of individual tryptophan residues, *Biophys. J.* 81 (2001) 1735–1758.
- [36] C. Rosen, G. Weber, Dimer formation from 1-amino-8-naphthalenesulfonate catalyzed by bovine serum albumin. A new fluorescent molecule with exceptional binding properties, *Biochemistry* 8 (1969) 3915–3920.
- [37] Q. Xie, H.M. Zhou, Refolding intermediate of guanidine hydrochloride denatured aminoacylase, *Int. J. Biochem. Cell Biol.* 36 (2004) 1332–1340.
- [38] T.B. Topping, L.M. Gloss, Stability and folding mechanism of mesophilic, thermophilic and hyperthermophilic archaeal histones: the importance of folding intermediates, *J. Mol. Biol.* 342 (2004) 247–260.
- [39] P.W. Riley, H. Cheng, D. Samuel, H. Roder, P.N. Walsh, Dimer dissociation and unfolding mechanism of coagulation factor XI apple 4 domain: spectroscopic and mutational analysis, *J. Mol. Biol.* 367 (2007) 558–573.
- [40] R. Jaenicke, H. Lilie, C.R. Matthews, Folding and association of oligomeric and multimeric proteins, *Adv. Protein Chem.* 53 (2000) 329–362.
- [41] H. Ke, S. Zhang, J. Li, G.J. Howlett, C.-C. Wang, Folding of *Escherichia coli* DsbC: characterization of a monomeric folding intermediate, *Biochemistry* 45 (2006) 15100–15110.
- [42] M. Baez, R. Cabrera, V. Guixe, J. Babul, Unfolding pathway of the dimeric and tetrameric forms of phosphofructokinase-2 from *Escherichia coli*, *Biochemistry* 46 (2007) 6141–6148.
- [43] J.K. Myers, C.N. Pace, J.M. Scholtz, Denaturant m values and heat capacity changes: relation to changes in accessible surface areas of protein unfolding, *Protein Sci.* 4 (1995) 2138–2148.
- [44] I.M. Kuznetsova, O.V. Stepanenko, K.K. Turoverov, L. Zhu, J.-M. Zhou, A.L. Fink, V.N. Uversky, Unraveling multistate unfolding of rabbit muscle creatine kinase, *Biochim. Biophys. Acta* 1596 (2002) 138–155.
- [45] I. Sakane, M. Ikeda, C. Matsumoto, T. Higurashi, K. Inoue, K. Hongo, T. Mizobata, Y. Kawata, Structural stability of oligomeric chaperonin 10: the role of two  $\beta$ -strands at the N and C termini in structural stabilization, *J. Mol. Biol.* 344 (2004) 1123–1133.
- [46] P. Sacchetta, A. Pennelli, T. Bucciarelli, L. Cornelio, F. Amicarelli, M. Miranda, C. Di Ilio, Multiple unfolded states of glutathione transferase bbGSTP1-1 by guanidinium chloride, *Arch. Biochem. Biophys.* 369 (1999) 100–106.
- [47] P.R. Louzada, A. Sebollela, M.E. Scaramello, S.T. Ferreira, Predissociated dimers and molten globule monomers in the equilibrium unfolding of yeast glutathione reductase, *Biophys. J.* 85 (2003) 3255–3261.
- [48] Y. Hagihara, S. Aimoto, A.L. Fink, Y. Goto, Guanidine hydrochloride-induced folding of proteins, *J. Mol. Biol.* 231 (1993) 180–184.
- [49] H.-R. Wang, T. Zhang, H.-M. Zhou, Comparison of inactivation and conformational-changes of aminoacylase during guanidinium chloride denaturation, *Biochim. Biophys. Acta, Prot. Struct. Mol. Enzymol.* 1248 (1995) 97–106.
- [50] M. Assfalg, L. Banci, I. Bertini, P. Turano, P.R. Vasos, Superoxide dismutase folding/unfolding pathway: role of the metal ions in modulating structural and dynamical features, *J. Mol. Biol.* 330 (2003) 145–158.
- [51] J.A. Tainer, E.D. Getzoff, K.M. Beem, J.S. Richardson, D.C. Richardson, Determination and analysis of the 2 Å structure of copper, zinc superoxide dismutase, *J. Mol. Biol.* 160 (1982) 181–217.
- [52] R.W. Strange, S. Antonyuk, M.A. Hough, P.A. Doucette, J.A. Rodriguez, P.J. Hart, L.J. Hayward, J.S. Valentine, S.S. Hasnain, The structure of holo and metal-deficient wild-type human Cu, Zn superoxide dismutase and its relevance to familial amyotrophic lateral sclerosis, *J. Mol. Biol.* 328 (2003) 877–891.
- [53] G. Mei, A. Di Venere, N. Rosato, A. Finazzi-Agro, The importance of being dimeric, *FEBS J.* 272 (2005) 16–27.
- [54] R. Jaenicke, Protein folding: local structures, domains, subunits, and assemblies, *Biochemistry* 30 (1991) 3147–3161.